J Neurophysiol 96: 826–833, 2006.
First published April 26, 2006; doi:10.1152/jn.00134.2006.

Models and Properties of Power-Law Adaptation in Neural Systems

Patrick J. Drew and L. F. Abbott

Neurobiology Section 0357, Division of Biology, University of California at San Diego, La Jolla, California; and Center for Neurobiology and Behavior, Department of Physiology and Cellular Biophysics, Columbia University College of Physicians and Surgeons, New York, New York

Submitted 8 February 2006; accepted in final form 23 April 2006

Drew, Patrick J. and L. F. Abbott. Models and properties of power-law adaptation in neural systems. *J Neurophysiol* 96: 826–833, 2006. First published April 26, 2006; doi:10.1152/jn.00134.2006. Many biological systems exhibit complex temporal behavior that cannot be adequately characterized by a single time constant. This dynamics, observed from single channels up to the level of human psychophysics, is often better described by power-law rather than exponential dependences on time. We develop and study the properties of neural models with scale-invariant, power-law adaptation and contrast them with the more commonly studied exponential case. Responses of an adapting firing-rate model to constant, pulsed, and oscillating inputs in both the power-law and exponential cases are considered. We construct a spiking model with power-law adaptation based on a nested cascade of processes and show that it can be "programmed" to produce a wide range of time delays. Finally, within a network model, we use power-law adaptation to reproduce long-term features of the tilt aftereffect.

INTRODUCTION

Activity-dependent plasticity and adaptation affect the characteristics of synapses and neurons over time scales ranging from milliseconds to minutes, or even longer, through a wide variety of mechanisms. Nevertheless in most studies, synaptic plasticity and neuronal response adaptation are analyzed and modeled using one or at most a few exponential processes, each characterized by a single time constant (see, however, Gilboa et al. 2005). It is typically impractical to model in detail the full range of processes and time constants suggested by experiment. A more reasonable alternative is to use power-law rather than exponential functions to describe the relevant dynamics. Power laws often provide an excellent and compact approximation in cases where multiple exponential processes are at play (Anderson 2001), and they have been used successfully to describe adaptation in neural systems (Thorson and Biderman-Thorson 1974). Most importantly, power-law descriptions allow the implications of the enormous range in time scales characteristic of plasticity and adaptation to be evaluated.

Power-law or multi- rather than single-exponential dependences on time are observed in biological systems ranging from single channels up to the level of human psychophysics. Power-law or multi-time-scale dynamics is found at the level of single-ion channels in studies of inactivation (Liebovitch et al. 1987; Millhauser et al. 1988; Toib et al. 1998), at the synaptic level in studies of short-term synaptic plasticity (Zucker and Regehr 2002), at the neuronal level in adaptation to various stimuli (Fairhall et al. 2001a,b; La Camera et al. 2004; Schwindt et al. 1989, 1992; Spain et al. 1991a,b; Xu et al. 1996), at the level of circuits in retinal sensitivity to contrast (Baccus and Meister 2002) and in auditory processing (Nelkin et al. 2003; Ulanovsky et al. 2003, 2004), and in the spectrum of local field potentials in visual cortex of both behaving and quiescent monkeys (Leopold et al. 2003). Xu, Payne, and Nelson (1996) found that adaptation in the firing rate of electroreceptors in electric fish was well fit by an inverse logarithmic function or by a power law. Response properties of the large-field motion-selective H1 neurons of flies display power-law dynamics (Fairhall et al. 2001a,b) and, similarly, the phase response properties of neurons in the vestibular system have been shown to correspond to fractional-order power-law behavior (Anastasio 1994; Oldham and Spanier 1974; Schneider and Anderson 1976; Si et al. 1997).

At the behavioral level, responses in many different cognitive tasks, from time estimation to drawing a line of a particular length, show power-law correlations (Gilden 2001; Gilden et al. 1995). In visual psychophysics, adaptation to contrast displays power-law dynamics (Magnussen and Greenlee 1985; Rose and Lowe 1982) as does the tilt aftereffect (Greenlee and Magnussen 1987). Memories are forgotten as a power law of time (Wixted and Ebbesen 1997), and synaptic plasticity with multiple timescales is more resistant to degradation by background activity than conventional single-time-scale plasticity (Fusi et al. 2005).

It is important to appreciate that we are not attempting to distinguish between power-law dynamics, when adaptation is described precisely by a power-law dependence on time, and multi-time-scale dynamics, when it is described by a sum of a large number of exponential processes with a range of time constants. Making such a distinction is purely academic because no experiment done over a finite time period can make it for us. Instead, we wish to develop models that describe either perfect power-law behavior or approximate power-law behavior arise from many underlying exponential processes, explore the resulting properties and contrast them with those found in simpler single-exponential models.

RESULTS

We begin our analysis of power-law dynamics by considering a general model of adaptation, which allows us to compare three forms: perfect, exponential, and power law. We study the

Address for reprint requests and other correspondence: P. J. Drew, Neurobiology Section 0357, Division of Biology, University of California at San Diego, 9500 Gilman Dr., La Jolla, CA 92093 (E-mail: pjdrew@biomail.ucsd.edu).

The costs of publication of this article were defrayed in part by the payment of page charges. The article must therefore be hereby marked "*advertisement*" in accordance with 18 U.S.C. Section 1734 solely to indicate this fact.

0022-3077/06 $8.00 Copyright © 2006 The American Physiological Society

Downloaded from jn.physiology.org on July 13, 2006

neural responses to constant, pulsed, and sinusoidal stimuli in the presence of these three forms of adaptation and compare them to results from fish electrosensory (Xu et al. 1996) and fly visual (Fairhall et al. 2001a,b) neurons. We also construct a model based on an integrate-and-fire neuron with an afterhyperpolarization current generated by a cascade process as a more practical and biophysically plausible instantiation of power-law adaptation. Finally, these models are used to produce programmable time delays and, in a network context, to account for data on the onset and recover of the visual tilt aftereffect (Greenlee and Magnussen 1987).

Different forms of adaptation

Generically, models of adaptation consist of an element that integrates the response of a system and feeds back the integrated signal to suppress that response (Fig. 1). We consider a simple case where the response $r(t)$ is linearly related to the stimulus $s(t)$, and the output of the suppressing integrator $I(t)$ has a subtractive effect on the response, so that $r(t) = s(t) - I(t)$. Because firing rates cannot be negative, the right side of this equation should really be rectified, but we do not consider any cases where negative rates arise even without rectification. Within this general framework, different types of adaptation are characterized by different forms of integration.

The most obvious operation for the adaptation integrator is an ordinary mathematical integration of the response

$$I(t) = \frac{1}{\tau_a}\int_0^t dt' r(t')$$

assuming that the response starts at time *0* (which we do throughout). This form of integration produces what is knows as perfect adaptation (Yi et al., 2000), which is equivalent to generating the response by high-pass filtering the stimulus. The parameter τ_a, which has the units of time, acts as the filter time constant. In perfect adaptation, the effects of a response are never "forgotten," they last forever, and the response to a constant stimulus invariably goes to zero. For these reasons, the model is not standard in neuroscience, and we will not consider it extensively, but it is nonetheless useful to introduce for comparison purposes.

Most models of neuronal adaptation use a leaky integrator with a finite lifetime in which

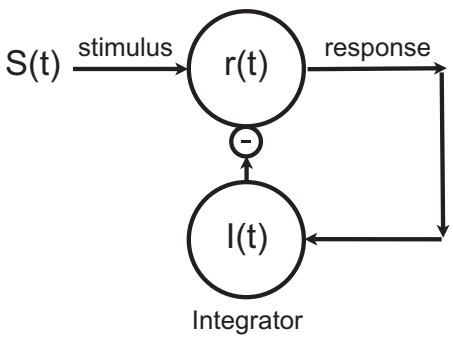

FIG. 1. A general model of adaptation. The stimulus $s(t)$ generates a response $r(t)$ that feeds back into an integrator $I(t)$. The integrator suppresses the response, so that $r(t) = s(t) - I(t)$. Different forms of adaptation correspond to different types of integrators.

$$I(t) = \frac{1}{\tau_a}\int_0^t dt' r(t') \exp((t' - t)/\tau_{ex})$$

This corresponds to the suppressive effect of the response being accumulated with exponential forgetting characterized by a time constant τ_{ex}. Perfect adaptation is the $\tau_{ex} \rightarrow \infty$ limit of this exponential form of adaptation.

We propose that data on neuronal adaptation suggests a form of power-law integration intermediate between perfect and exponential, in which

$$I(t) = \alpha\int_0^t dt' \frac{r(t')}{t - t' + \beta}$$

Here α is a dimensionless constant and β is a parameter with units of time. In this case, the suppressive effects of the response are accumulated with power-law, rather than exponential, forgetting. The much longer "tail" on the power-law function compared with the exponential produces a longer memory for past responses, although not the complete memory of perfect adaptation. In addition, the fact that the parameter α, which controls the magnitude of the adaptation, is dimensionless in this case (whereas the analogous factor $1/\tau_a$ for the other forms has the dimensions of a frequency) gives this form of adaptation the interesting feature of scale-invariance.

To compare and contrast these three forms of adaptation, we consider cases in which $s(t)$ is constant for all positive times, consists of a square pulse, or varies sinusoidally.

Response to constant stimulus

As mentioned in the preceding text, responses to constant stimuli inevitably go to zero over time with perfect adaptation. With exponential adaptation, activation of a stimulus that then remains constant produces a transient response that decays exponentially to a nonzero, steady-state value of $\tau_a s/(\tau_a + \tau_{ex})$ with time constant $\tau_{eff} = \tau_a\tau_{ex}/(\tau_a + \tau_{ex})$. The blue lines in Fig. 2*A* show this transient/sustained response when $\tau_a = 200$ ms and $\tau_{ex} = 1$ s, plotted over three different time scales.

Like perfect adaptation, the scale-invariant form of power-law adaptation does not allow the response to a constant stimulus to remain nonzero indefinitely. Although there is forgetting, it is weak enough to make the adaptation integral grow without bound if the response is held constant. However, this divergence is only logarithmic, so the approach to zero response is extremely slow. As a result, over any particular time period this form of adaptation can look qualitatively similar to exponential adaptation. For example, the red (power-law adaptation with α and $\beta = 50$ ms) and blue (exponential) curves in Fig. 2*A, top,* appear to show the same general trends. The difference between these two forms of adaptation only becomes apparent when the effect is plotted over different time intervals, as in Fig. 2*A, bottom two panels*. In exponential adaptation, the transition between the initial transient and the later sustained responses occurs over a fixed time interval and thus appears sharper when plotted on a 10-fold expanded time scale. On the other hand, the red curves depicting the response with power-law adaptation have a similar shape in all three panels of Fig. 2*A*, particularly in the *bottom two.* This is an example of the scale-invariant property of power-law adaptation.

Downloaded from jn.physiology.org on July 13, 2006

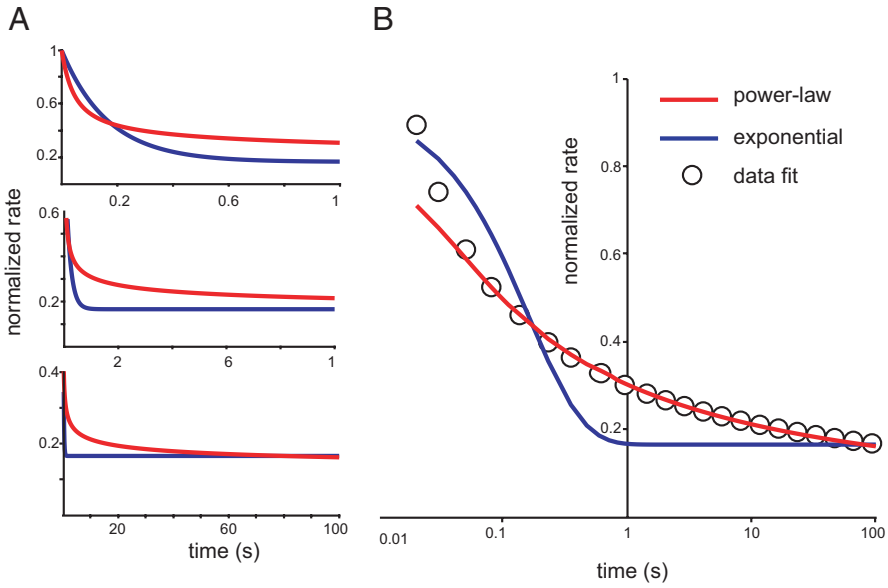

FIG. 2. Time courses of firing rates in response to constant input for exponential (blue curves) and power-law (red curves) adaptation. *A*: firing rates, normalized to a maximum value of 1, plotted over 3 different time scales. *B*: normalized firing rates plotted on a logarithmic time axis and compared with the data fit of Xu, Payne, and Nelson (1996), denoted by open circles.

The scale invariance of the power-law adaptation seen in Fig. 2*A* challenges some of the basic assumptions commonly made about adaptation. Figure 2*A, top,* alone (red curve) would suggest that we are seeing a transient response lasting ~100 ms, followed by a roughly constant sustained plateau. From the *middle panel* alone, we might conclude that the transient response lasts for ~1 s before the constant plateau sets in. The *bottom panel* alone would indicate that we were looking at a 10-s transient followed by a sustained response. None of these views is correct. In fact, power-law adaptation challenges the standard language used to describe adaptation phenomena because it has no well-defined transient and sustained components. Instead, if a conventional split into transient and sustained components is forced on the data, the nature of the division will depend on the duration of the experiment. Similarly, the value of any time constant extracted to describe the adaptation will depend on the duration of the experiment being fit.

Responses arising from exponential and power-law adaptation are compared with each other and with a data fit to responses of electrosensory neurons in the electric fish (Xu et al. 1996) over a logarithmic time axis in Fig. 2*B*. Xu, Payne, and Nelson (1996) fit their data on adaptation using the equation $r(t) = A/[1 + B\ln(t)]$, where t is in units of seconds, A is a constant ~100 Hz, and B is between 0.1 and 0.2 (in reality, these authors describe a change in firing rate not the absolute firing rate, but, for simplicity, we ignore background firing). In Fig. 2*B*, we show the example with $B = 0.17$ shown in Fig. 4 of their paper, on which our Fig. 2 is based (in our plot, $A = 0.3$ because we have normalized the firing rate to an initial value of 1). Obviously, the exponential (blue) curve cannot fit these data with the parameters used for Fig. 2, and it cannot fit it for another set of parameters either. The exponential curve simply has the wrong shape.

The model of power-law adaptation we are studying matches the data fit for times ranging from 20 ms to 100 s after stimulus onset (red curve in Fig. 2*B*). In this particular case, the power-law model underestimates the amount of adaptation below ~20 ms. Note that we are comparing our model to a fit of the data in Xu, Payne, and Nelson (1996), which they report to be excellent, not to the data itself (we refer the reader to the original paper for a description of the data). The values of the parameter B used to fit these data ranged between 0.1 and 0.2 for different neurons. The power-law model matches well when $B < 0.15$, which occurs in ~50% of cases studied by Xu, Payne, and Nelson (1996). For larger B values, as in Fig. 2*B*, there is an underestimation of adaptation at short times, suggesting that an additional, short-lasting exponential form of adaptation may also contribute in these cases. In the following, we are interested in exploring consequences of the longer-lasting effects of adaptation, and for this purpose, we consider the power-law model an adequate fit, even if it sometimes underestimates short-term effects as in Fig. 2*B*. The power-law form of adaptation we are using is similar to the logarithmic form chosen by Xu, Payne, and Nelson (1996) because, over most of the time range, the firing rate changes quite slowly. In this case, the integral of the power-law adaptation kernel times the firing rate is logarithmic to a good approximation.

Response to pulsed stimulus

We now consider a pulsed stimulus so that we can study recovery from adaptation. To illustrate recovery, we plot the value of the adaptation integral $I(t)$ rather than the response itself because the response simply goes to zero when the stimulus pulse terminates. Figure 3*A* compares onset and recovery dynamics for exponential (blue curve) and power-law (red curve) forms of adaptation using the same parameters as in Fig. 2. As before, the two forms look qualitatively similar if they are examined over a single time range, as in Fig. 3*A, top*. However, a comparison of the two panels in Fig. 3*A*, which shows the effects of square-wave stimulus pulses lasting for 5 (*top*) and 50 s (*bottom*), illustrates another aspect of the scale-invariance of power-law adaptation. Whereas the exponential adaptation integral recovers back to zero over a fixed time period of order τ_{eff} irrespective of the duration of the stimulus pulse, the rate of recovery for the power-law model is proportional to the duration of the pulse. This can be seen because the red curves indicating recovery after the 5-s pulse (*top*) and after the 50 s pulse (*bottom*) look almost identical

Downloaded from jn.physiology.org on July 13, 2006

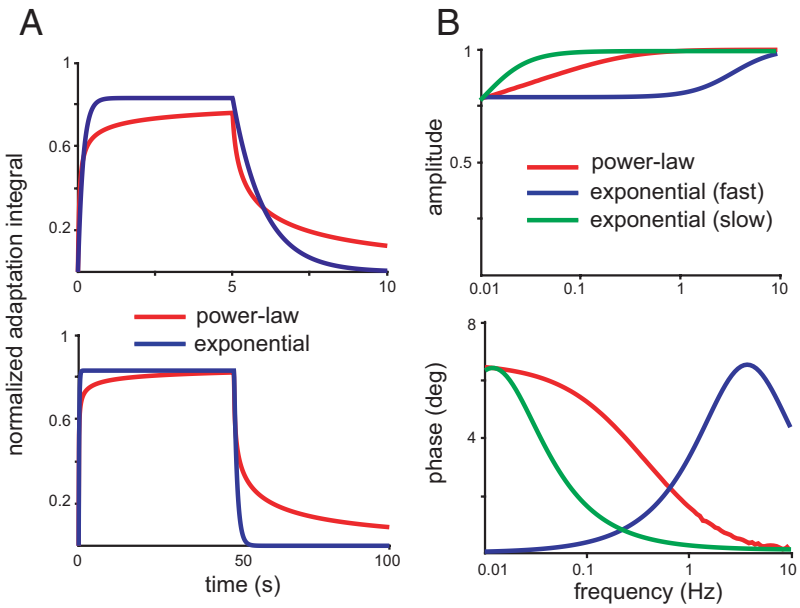

FIG. 3. Responses of exponential (blue curves) and power-law (red curves) adaptation models to pulsed and oscillatory inputs. *A*: adaptation integral in response to input pulses lasting for 5 s (*top*) and 50 s (*bottom*). *B*: relative amplitude and phase of the response to an oscillatory input at different frequencies, plotted on a logarithmic scale.

although they are plotted on time axes that differ by a factor of 10 (the same factor by which the pulse durations differ). Recovery time that varies with stimulus duration time is a defining feature of power-law adaptation (Fairhall et al. 2001a,b; Toib et al. 1998).

Response to oscillating stimulus

To further characterize power-law adaptation and to contrast it with exponential adaptation, we consider a sinusoidally varying stimulus

$$s(t) = s_0 + s_1 \cos(2\pi ft)$$

for different frequencies f, where s_0 and s_1 are constants (we take $s_0 > s_1$ to avoid negative responses). The response, in this case, can be characterized by an amplitude and phase. Before proceeding, however, we must face a complication associated with the power-law model of adaptation we are considering.

As mentioned in the preceding text, the adaptation integral in the power-law case diverges if the response remains constant over time. This divergence implies that the response to any stimulus with a nonzero time average will eventually go to zero. Although this approach is slow enough not to interfere with intuitive notions of response amplitude and phase, it does imply that they are not well defined mathematically. To avoid this problem, we introduce a finite cutoff into the adaptation integral, replacing it with the integral

$$I(t) = \alpha \int_{\max(0,t-T)}^{t} dt' \frac{r(t')}{t - t' + \beta}$$

The lower integration limit, which is 0 if $t - T \leq 0$ and $t - T$ otherwise, starts at the time of stimulus onset, and it never extends back in time more than an interval T into the past. We use $T = 1{,}000$ s. This imposes the reasonable biophysical constraint that the memory of past activity retained by the adaptation integral is finite. With this constraint imposed, the amplitude and phase are well defined, and we can proceed with the analysis.

The amplitude and phase are defined by writing the response to the sinusoidal stimulus as $r(t) = r_0 + r_1 \cos(2\pi ft + \delta)$. The amplitude plotted in Fig. 3*B* is the ratio r_1/s_1 and the phase is δ (although we plot it in degrees rather than radians).

Both exponential (blue and green curves) and power-law (red curve) forms of adaptation show partial high-pass filtering properties in Fig. 3*B, top*. However, the phase advances they produce (Fig. 3*B, bottom*) are quite different. Exponential adaptation with a short time constants ($\tau_a = 200$ ms and $\tau_{ex} = 50$ ms, blue curve) produces a phase shift that is sensitive to frequency and that vanishes in both the high- and low-frequency limits. When the time constants governing the exponential adaptation are much larger ($\tau_a = 60$ s and $\tau_{ex} = 15$ s, green curve), the phase shift curve moves to the left so that even the lowest frequency shown in Fig. 3*B* is associated with a nonzero phase advance. However, the phase shift falls rapidly to zero as the frequency is increased in this case. The phase shift in the exponential case always has a peak, and both the location of the peak and its width scale in the same way. Thus on the logarithmic plot of Fig. 3*B*, the phase shift curve shifts but does not broaden when τ_{ex} is varied, and it is not possible to maintain a roughly constant phase shift around the peak over a wide range of frequencies.

The phase shift for power-law adaptation (red curve) shares with the slow exponential, the property of having a nonzero phase shift at low frequencies, but the phase shift falls off much more slowly as the frequency is increased. For the lowest range of frequencies in Fig. 3*B*, the phase shift produced by power-law adaptation is relatively constant. Such behavior has been seen experimentally (Fairhall et al. 2001b), and it has some interesting consequences.

Frequency-independent phase shifts are the basis of the Hilbert transform that is widely used for signal, in particular auditory, processing (Hartman 1996). Frequency-independent phase shifts are also found in motor systems, allowing swimming motions, for example, to be made at different speeds (Cohen et al. 1992). Power-law adaptation may provide a solution to the long-standing puzzle of how to introduce constant phase rather than constant duration, lags and advances

Downloaded from jn.physiology.org on July 13, 2006

into motor pattern-generating networks (Abbott et al. 1991). The phase shifts shown in Fig. 3*B* are fairly small, but larger shifts can be obtained simply by increasing the parameter α (the value of α used in Fig. 3*B* was chosen to match previous figures).

Spiking model with power-law adaptation

The model analyzed in the previous section is general but fairly idealized. We now show how power-law adaptation can be implemented within a standard spiking neuron model. For this purpose, we consider an integrate-and-fire model neuron that fires an action potential whenever its membrane potential reaches a threshold of −50 mV, after which it is reset to −70 mV. Below threshold, the membrane potential satisfies

$$\tau_m \frac{dV}{dt} = V_{rest} - V - I + s$$

with $V_{rest} = -70$ mV and $\tau_m = 10$ ms. The current denoted by s represents the stimulus as in the preceding text. The current denoted by I, which plays the same role as the adaptation integral, is an afterhyperpolarization current that could be the result of calcium-activated potassium channels for example.

In a standard model of exponential adaptation, I might jump up by a certain amount following each action potential and decay exponentially between action potentials. To implement power-law adaptation, we retain the jump after an action potential, but we change the recovery dynamics between action potentials. The most direct way to do this is to express the adaptation current at time t following a sequence of n action potentials occurring at times $t_1, t_2, \ldots, t_n$ as

$$I(t) = \gamma \sum_{i=1}^{n} \frac{1}{t - t_i + \beta}$$

The similarity to the adaptation integral in the previous section should be apparent, with the parameter γ setting the level of adaptation just as α did before. This formulation does indeed reproduce the results shown in Figs. 2 and 3 within a spiking model, but it is fairly cumbersome to implement. For this reason, and to make contact with underlying mechanisms, we present an alternative formulation.

An inverse time dependence, as needed for the power-law adaptation integral, can always be approximated by a series of exponentials. However, there is a more efficient way of using a number of exponential processes to approximate power-law adaptation (Aurell et al. 1996; Hausdorff and Peng 1996; Peng et al. 1993). Rather than simply adding together a number of noninteracting exponential processes to reproduce the power-law forgetting in power-law adaptation, we link these process to each other. This allows us to accurately approximated the power-law with fewer elements and computations. Consider N processes, described by dynamic variables z_i obeying $\tau_i(dz_i/dt) = z_i + z_{i+1}$ for $i = 1, 2, \ldots, N$, with $z_{N+1} \equiv 0$ and $\tau_i = \tau_1 \delta^{i-1}$ for some value of $\delta > 1$. This corresponds to a cascade of processes in which the equilibrium point of process i is determined by process $i + 1$. Immediately after each action potential, we impose jumps $z_i \rightarrow z_i + \gamma\delta^{1-i}$ on all N variables, where the parameter γ controls the degree of adaptation. This corresponds to adding an impulse (delta function) term to the equations for the z_i with a strength proportional to τ_i. If we set the adaptation current $I = z_1$ in this scheme, we accurately reproduce power-law adaptation with $\beta = (N - 1)\tau_1 / \ln(\tau_N/\tau_1)$ over times ranging from τ_1 up to approximately $\tau_N/(\delta - 1)$.

Figure 4 shows a comparison of the general model (red curve) and data fit (open circles) seen in Fig. 2 with the results of the integrate-and-fire model (green dots) described in the preceding text with an adaptation current controlled by $N = 495$ cascade processes with $\tau_1 = 1$ ms, $\tau_{495} = 1{,}000$ s, and $\gamma = 1.25$ mV. The firing rate for the integrate-and-fire model responding to a constant input current is plotted at the time of a spike and is one over the time since the previous spike. There is some difference between the firing rate of the general model and that of the integrate-and-fire model for the initial spikes, probably due to the ambiguity of this definition of firing rate, but over the range from 20 ms to 100 s seen in Fig. 4, the match is excellent.

Programmable time delays

A good example of the utility of scale-invariant adaptation is provided by considering a neuron that acts as a programmable timer. If a neuron with a power-law adaptation a rate r for a time T, the adaptation integral at subsequent times is given by

$$I(t) = \alpha r \int_0^T dt' \frac{1}{t - t' + \beta} = \alpha r \ln\left(\frac{t + \beta}{t - T + \beta}\right) \approx \frac{\alpha r' T}{t}$$

where the approximate equality $t \gg \beta$ and $t \gg T$. Imagine that we have a neuron that fires at a rate $r(t) = s_0 - I(t)$ whenever the adaptation current is less than some threshold value s_0. If we activate such a neuron at a high enough rate r for a sufficiently long time T to make $I > s_0$, it will resume firing at a time given by $I(t) = s_0$ or, from the preceding equation, $t = \alpha r T / s_0$. If α is of order 1 and s_0 is fairly small, this can easily exceed 100 times the duration of the period over which the adaptation was established. This allows a neuron with a scale-invariant adaptation current to act as a rapidly programmable timer.

Figure 5*A* shows an illustration of the integrate-and-fire model with cascade-driven adaptation current described in the previous section acting in this manner. In all three cases, a constant current just above threshold keeps that neuron firing at a low rate initially. Then at time $t = 20$ s, current pulses lasting for $T = 1$ s were used to drive the neuron at various rates. This resulted in pauses in the firing of various durations that depend

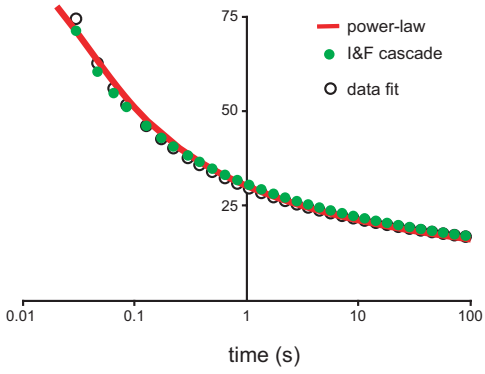

FIG. 4. Comparison of the firing rates of the general model (red curve) and the data fit (open black circles) of Fig. 2 with an integrate-and-fire model (green dots) with an adaptation current generated by a cascade of exponential processes.

Downloaded from jn.physiology.org on July 13, 2006

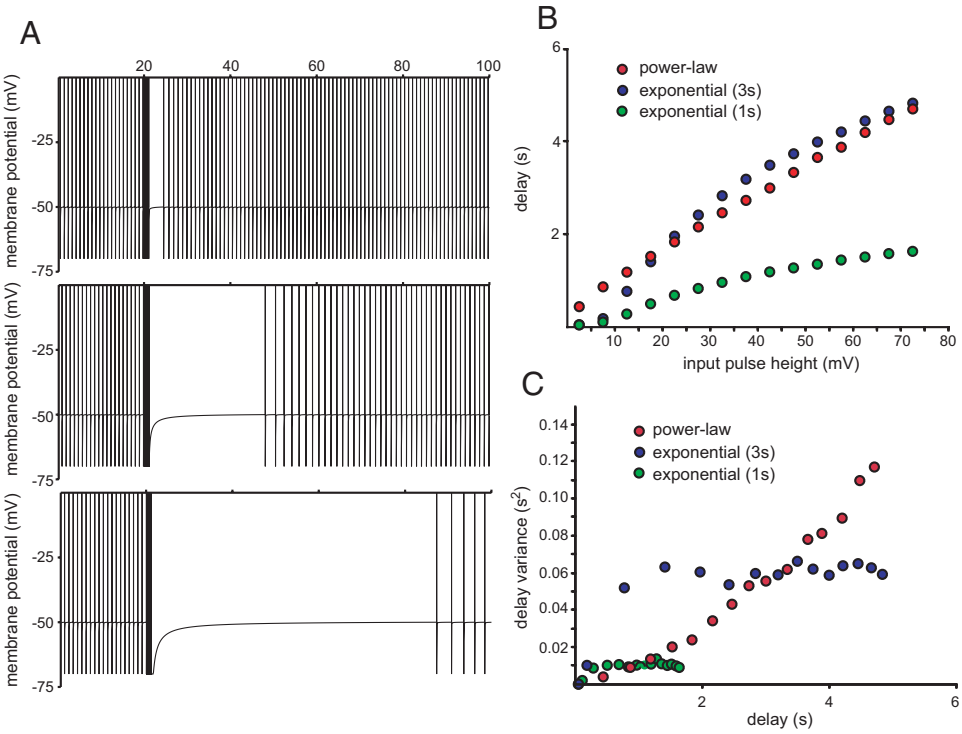

FIG. 5. Programmable time delays. A spiking model with power-law adaptation and a constant background firing rate is excited by a current pulse lasting either 1 s (*A*) or 0.2 s (*B* and *C*). *A*: voltage trace of the spiking model neuron. Depending on the magnitude of the current pulse, different firing delay intervals can be obtained. *B*: firing delays as a function of the amplitude of a 200 ms injected current at beginning of the trial. Current amplitude, measured in mV, reflects the amount of steady-state depolarization that this amplitude of current would produce with spiking turned off (infinite threshold). Gaussian noise with a SD of 2 mV was injected throughout. *C*: variance of the time delays in *B*. In *B* and *C*, red points show the power-law model, blue dots show a spiking model with exponential adaptation with τ_{ex} = 3 s and green dots show exponential adaptation with τ_{ex} = 1 s, with spike-evoked increments of 0.05 and 0.15, respectively.

linearly on the amplitude of the current pulse (red points, Fig. 5*B*).

A neuronal timer that uses scale-invariant adaptation is well buffered against error over its entire range, in sharp contrast to a timer that uses exponential adaptation (see following text). Noting that the quantity rT is the number of action potentials, N, fired during the timer-setting period, we can write the duration of the timed delay as $t = \alpha N/s_0$. Suppose that there is an error ΔN in the number of action potentials used to set the delay or there is an error Δs_0 in the value of the threshold for firing. A first-order Taylor expansion shows that in these cases, the resulting error Δt in the duration of the delay interval is given by $\Delta t/t = \Delta N/N$ or $\Delta t/t = \Delta s_0/s_0$. In other words, the size of the error is proportional to the size of the time interval with the constant of proportionality given by the fractional error in the number of spikes or threshold. Thus a 10% error in either the setting or the thresholding conditions produces a 10% error in the delay duration over the entire range of timed delays. This can be seen for the spiking-model timer shown in Fig. 5*A* and in the red points in Fig. 5*B*. To make this figure, we introduced noise into the spiking model by putting in Gaussian white noise with a SD of 2 mV. Each trial started with a 200-ms current pulse of varying intensity, after which the current was turned down to provide a 20.4-mV depolarization, enough to cause spiking. The delay between the end of the pulse and the first spike was recorded for 250 trials at each current pulse intensity. The mean and variance of the delay to the first spike are plotted in Fig. 5, *B* and *C*. As expected, the size of the variance for the power-law case (red points) grows with the size of the delay interval or, more importantly, shrinks as the decay interval gets smaller.

A timer based on exponential adaptation can only work over a range that is more restricted than with power-law adaptation. To avoid saturation of the adaptation in the exponential case, the forgetting time must much larger than the setting interval, $\tau_{ex} \gg T$. If this holds, the adaptation current after the setting pulse is given by

$$I(t) = \frac{r\tau_{ex}}{s_0\tau_a}\left(\exp(T/\tau_{ex}) - 1\right)\exp(-t/\tau_{ex}) \approx \frac{rT}{s_0\tau_a}\exp(-t/\tau_{ex})$$

and the duration of the subsequent delay is $t = \tau_{ex}\ln(rT/s_0\tau_a) = \tau_{ex}\ln(N/s_0\tau_a)$. This allows for delay intervals from zero up to a few times τ_{ex}. If τ_{ex} is too small (1 s), as for the green points in Fig. 5*B*, the delay intervals saturate as a function of the amplitude of the current injected during the setting interval. This problem appears to be resolved if, as for the blue points in Fig. 5*B*, τ_{ex} is taken to be large (3 s). However, the errors caused by deviations in the number of setting spikes or the threshold in this case are far more severe than in the power-law case. The same analysis applied in the previous paragraph gives, in this case, $\Delta t/\tau_{ex} = \Delta N/N$ or $\Delta t/\tau_{ex} = \Delta s_0/s_0$. This means that the error is always some fraction (say, 10%) of the time constant τ_{ex}, even for short delays. This makes short intervals inaccurate and restricts the exponential scheme to a small range of time intervals quite close to τ_{ex}. The constant-sized errors made in the exponential case can be seen in the blue and green points in Fig. 5*C*. Note that, for τ_{ex} = 1 s, saturation prevents long delays, and for τ_{ex} = 3 s, the errors get large for short time intervals. Either way, the range is much more restricted than for power-law adaptation.

Power-law adaptation in a network and the tilt aftereffect

As an example of using power-law adaptation in a network model to reproduce a known sensory phenomenon, we consider the tilt aftereffect. After prolonged adaptation to an oriented visual stimulus, human subjects perceive oriented test stimuli as been rotated away from the angle of the adapting stimulus. This is the tilt aftereffect. The long-term time course

Downloaded from jn.physiology.org on July 13, 2006

for the onset and recovery from the tilt effect is logarithmic (Greenlee and Magnussen 1987).

To consider the tilt aftereffect, we incorporated power-law adaptation into a standard network model of orientation tuning in visual cortex (Ben-Yishai et al. 1995) (see METHODS). The input to this model is characterized by an angle that corresponds to the orientation of a bar or grating image. The "perceived" orientation corresponding to this input is extracted from the network activity by a population vector technique (see METHODS). Initially, the input orientation angle and the decoded population angle are equal, reflecting accurate representation of the oriented stimulus. Prolonged exposure to a particular input angle, however, adapts neurons with strong responses to that angle, which distorts the population response to other input orientations and produces a tilt aftereffect. The magnitude and sign of the tilt aftereffect produced in this way depend on a number of factors (Dragoi et al. 2000; Jin et al. 2005; Kohn and Movshon 2004; Muller et al. 1999; Teich and Qian 2003). For the parameters we use, we find a tilt aftereffect of the correct sign, although the magnitude is larger than what is observed psychophysically. The point of our model is to examine the dynamics of onset and recovery not to accurate reproduce all aspects of the tilt illusion.

The tilt aftereffect in the network model is show in Fig. 6. The adapting stimulus and the test stimulus for this figures had orientations 12° apart. The aftereffect being plotted is the difference between the test stimulus and the decoded population activity (METHODS), with the convention that positive angles correspond to perceiving the test orientation rotated away from the adapting angle. The tilt aftereffect in the model depends on the duration of both the adaptation and the recovery. In Fig. 6, the decoding error is plotted as a function of time spent adapting (*left*), measured with a 500-ms gap between adapting and test stimuli, or the time spent recovering from 15 s of adaptation (*right*). In contrast to a network of exponentially adapting neurons, which shows saturation and recovered after a few time constants, the power-law adapting network shows that the onset and offset of the error show a logarithmic, nonsaturating, dependence as is seen in the psychophysical data (Greenlee and Magnussen 1987).

Rather than arising from neuronal adaptation, the tilt aftereffect in this network model could arise from synaptic depression or both could contribute. We have tested the same network model with power-law synaptic depression (which is a divisive rather than subtractive effect) and obtained similar results to the adaptation model. We chose to show the case of neuronal adaptation because there is evidence of power-law adaptation of this type in a primary sensory cortical area, although auditory rather than visual (Ulanovsky et al. 2004).

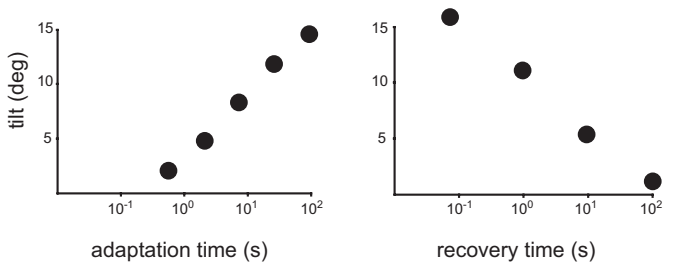

FIG. 6. Strength of the tilt aftereffect as a function of adaptation and recovery time. *Left*: magnitude of the tilt aftereffect in a network model as a function of the presentation time of the adapting stimulus. *Right*: recovery from adaptation after a 15-s presentation of the adapting stimulus, measured after recovery periods of different length (horizontal axis). Both cases show a logarithmic dependence on time, matching psychophysical studies (Greenlee and Magnussen 1987).

DISCUSSION

We have considered adaptation with different forms of stimulus history dependence, focusing in particular on the power-law case. In perfect adaptation, the entire response history is retained forever by the adaptation mechanisms. With exponential adaptation, activity more than a few time constants back is effectively forgotten, and only the relatively recent past contributes. Power-law adaptation is an intermediate case with past activity discounted but not forgotten. Power-law adaptation is a temporal "generalist" in that it can act over a range of time scales. This is advantageous for an organism that has to deal with natural stimuli that vary on multiple time scales.

Power-law dynamics can arise in a number of ways (Henry and Wearne 2000). The fact that we can mimic power-law adaptation, at least over a finite time interval, using a sum or cascade of exponential functions means that it could arise simply from a large number of processes exhibiting ordinary exponential dynamics but with a wide range of time constants. Indeed, where the biophysics of neuronal firing rate adaptation has been studied in detail, multiple contributing processes have been found (Schwindt et al., 1989, 1992; Spain et al. 1991ab). Multiple processes often contribute to biological systems where, at first sight, one would appear to suffice. We suggest that this multiplicity may arise from the need for power-law dynamics.

Natural stimuli vary over an extremely wide range of time scales, and it is difficult to predict what stimulus durations will be encountered in any given situation. Having a fixed recovery time, as in exponential adaptation, seems a poor way to deal with such variety. Instead, it makes sense to let the temporal statistics of the stimuli being encountered set the dynamics of the adaptation being used to process them. Power-law adaptation allows such flexibility to arise automatically from basic properties of the adaptation process.

MODELS

The adapting models used are included in the text. Here we describe the network model used for Fig. 6. The firing rates of individual neurons in the network are given by the equation

$$\tau_r \frac{dr_i(t)}{dt} = -r_i(t) + [A_i(t)]_+$$

where $r_i(t)$ is the firing rate of a neuron with unadapted orientation preference for angle θ_i, the brackets denote rectification, and $\tau_r = 5$ ms. The current for neuron i, $A_i(t)$, is given by

$$A_i(t) = C\left[1 - \varepsilon + \varepsilon \cos(\theta_i - \theta_{input})\right] + \frac{1}{N}\sum_{j=1}^{N} J_2 \cos(\theta_i - \theta_j) r_j(t) - I_i(t)$$

where θ_{input} is the input angle corresponding to the stimulus orientation, $C = 50$ Hz is proportional to the stimulus contrast, $\varepsilon = 0.5$ is the tuning specificity of the feed-forward input, the recurrent strength J_2 was set to 2.0, and $I_i(t)$ is the adaptation current. The adaptation current for a given neuron is described

Downloaded from jn.physiology.org on July 13, 2006

by a convolution of a power-law kernel with its prior activity level

$$I_i(t) = \alpha \int_0^t dt' \frac{r_i(t')}{t - t' + \beta}$$

with $\alpha = 5$ Hz and $\beta = 2.7$ ms.

The output of the network was decoded used a vector sum decoding method

$$\theta_{pop} = \arctan\left[\frac{\sum_{i=1}^{N} r_i \sin(2\pi\theta_i)}{\sum_{i=1}^{N} r_i \cos(2\pi\theta_i)}\right]$$

In simulations, the population orientation angle θ_{pop} was averaged over a 50-ms test stimulus.

ACKNOWLEDGMENTS

We thank S. Fusi for helpful discussions.

GRANTS

This research was supported by National Institute of Mental Health Grant MH-58754, the Swartz Foundation, and an NIH Director's Pioneer Award, part of the NIH Roadmap for Medical Research, through grant number 5-DP1-OD114-02.

REFERENCES

Abbott LF, Marder E, and Hooper SL. Oscillating networks: control of burst duration by electrically coupled neurons. *Neural Comp* 3: 487–497, 1991.

Anastasio TJ. The fractional-order dynamics of brain-stem vestibulooculomotor neurons. *Biol Cybern* 72: 69–79, 1994.

Anderson RB. The power law as an emergent property. *Mem Cognit* 29: 1061–1068, 2001.

Aurell E, Boffetta G, Crisanti A, Paladin G, and Vulpiani A. Predictability in systems with many characteristic times: the case of turbulence. *Phys Rev* E 53: 2337–2349, 1996.

Baccus S and Meister M. Fast and slow contrast adaptation in retinal circuitry. *Neuron* 36: 909–919, 2002.

Ben-Yishai R, Bar-Or RL, and Sompolinsky H. Theory of orientation tuning in visual cortex. *Proc Natl Acad Sci USA* 92: 3844–3848, 1995.

Cohen AH, Ermentrout GB, Kiemel T, Kopell H, Sigvartdt KA, and Williams TL. Modelling of intersegmental coordination in the lamprey central pattern generator for locomotion. *Trends Neurosci* 15: 434–438, 1992.

Dragoi V, Sharma J, and Sur M. Adaptation-induced plasticity of orientation tuning in adult visual cortex. *Neuron* 28: 287–298, 2000.

Fairhall AL, Lewen GD, Bialek W, and de Ruyter van Steveninck RR. Efficiency and ambiguity in an adaptive neural code. *Nature* 412: 787–792, 2001a.

Fairhall AL, Lewen GD, Bialek W, and de Ruyter van Steveninck RR. Multiple time scales of adaptation in a neural code. *Adv Neural Inform Proc Syst* 13: 124–130, 2001b.

Fusi S, Drew PJ, and Abbott LF. Cascade models of synaptically stored memories. *Neuron* 45: 599–611, 2005.

Gilboa G, Chen R, and Brenner N. History-dependent multiple time scale dynamics in a single neuron model. *J Neurosci* 25: 6479–6489, 2005.

Gilden DL. Cognitive emissions of 1/f noise. *Psychol Rev* 108: 33–56, 2001.

Gilden DL, Thornton T, and Mallon MW. 1/f noise in human cognition. *Science* 267: 1837–1839, 1995.

Greenlee MW and Magnussen S. Saturation of the tilt aftereffect. *Vision Res* 27: 1041–1043, 1987.

Hartman W. *Signals, Sound, and Sensation.* Berlin: Springer-Verlag, 1996.

Hausdorff JM and Peng C-K. Multiscaled randomness: a possible source of 1/f noise in biology. *Phys Rev* E 54: 2154–2157, 1996.

Henry BI and Wearne SL. Fractional reaction-diffusion. *Physica* A 276: 448–455, 2000.

Jin DZ, Dragoi V, Sur M, and Seung HS. The tilt aftereffect and adaptation-induced changes in orientation tuning in visual cortex. *J Neurophysiol* 94: 4038–4050, 2005.

Kohn A and Movshon JA. Adaptation changes the direction tuning of MT neurons. *Nat Neurosci* 7: 764–772, 2004.

La Camera G, Rauch A, Luscher HR, Senn W, and Fusi S. Minimal models of adapted neuronal response to in-vivo-like input currents. *Neural Comput* 16: 2101–2124, 2004.

Leopold DA, Murayama Y, and Logothetis N. Very slow activity fluctuations in monkey visual cortex: implications for functional brain imaging. *Cereb Cortex* 13: 422–433, 2003.

Liebovitch LS, Fischbarg J, Koniarek JP, Todorova I, and Wang M. Fractal model of ion-channel kinetics. *Biochim Biophys Acta* 896: 173–180, 1987.

Magnussen S and Greenlee MW. Marathon adaptation to spatial contrast: saturation in sight. *Vision Res* 25: 1409–1411, 1985.

Millhauser GL, Salpeter EE, and Oswald RE. Diffusion models of ion-channel gating and the origin of power-law distributions from single-channel recording. *Proc Natl Acad Sci USA* 85: 1503–1507, 1988.

Muller JR, Metha AB, Krauskopf J, and Lennie P. Rapid adaptation in visual cortex to the structure of images. *Science* 285: 1405–1408, 1999.

Nelken I, Fishbach A, Las L, Ulanovsky N, and Farkas D. Primary auditory cortex of cats: feature detector or something else? *Biol Cybern* 89: 397–406, 2003.

Oldham KB, Spanier J. *The Fractional Calculus.* New York: Academic, 1974.

Peng C-K, Mietus J, Hausdorff JM, Havlin S, Stanley HE, and Goldberger AL. Long-range anticorrelations and non-Gaussian behavior of the heartbeat. *Phys Rev Lett* 70: 1343–1346, 1993.

Rose D and Lowe I. Dynamics of adaptation to contrast. *Perception* 11: 505–528, 1982.

Schwindt PC, Spain WJ, and Crill WE. Long-lasting reduction of excitability by a sodium-dependent potassium current in cat neocortical neurons. *J Neurophysiol* 61: 233–244, 1989.

Schwindt PC, Spain WJ, and Crill WE. Calcium-dependent potassium currents in neurons from cat sensorimotor cortex. *J Neurophysiol* 67: 216–226, 1992.

Schneider LW and Anderson DJ. Transfer characteristics of first and second-order lateral canal vestibular neurons in gerbel. *Brain Res* 112: 61–72, 1976.

Si XH, Angelaki DE, and Dickman JD. Reponse properties of pigeon otolith afferents to linear acceleration. *Exp Brain Res* 117: 242–250, 1997.

Spain WJ, Schwindt PC, and Crill WE. Post-inhibitory excitation and inhibition in layer V pyramidal neurons from cat sensorimotor cortex. *J Physiol* 434: 609–626, 1991a.

Spain WJ, Schwindt PC, and Crill WE. Two transient potassium currents in layer V pyramidal neurons from cat sensorimotor cortex. *J Physiol* 434: 591–607, 1991b.

Teich A and Qian N. Learning and adaptation in a recurrent model of V1 orientation selectivity. *J Neurophysiol* 89: 2086–2100, 2003.

Thorson J and Biederman-Thorson M. Distributed relaxation processes in sensory adaptation. *Science* 183: 161–172, 1974.

Toib A, Lyakhov V, and Marom S. Interaction between duration of activity and time course of recovery from slow inactivation in mammalian brain Na^+ channels. *J Neurosci* 18: 1893–1903, 1998.

Ulanovsky N, Las L, Farkas D, and Nelken I. Multiple time scales of adaptation in auditory cortex neurons. *J Neurosci* 24: 10440–10453, 2004.

Ulanovsky N, Las L, and Nelken I. Processing of low-probability sounds by cortical neurons. *Nat Neurosci* 6: 391–398, 2003.

Wixted JT and Ebbesen E. Genuine power curves in forgetting. *Mem Cognit* 25: 731–739, 1997.

Xu Z, Payne JR, and Nelson ME. Logarithmic time course of sensory adaptation in electrosensory afferent nerve fibers in a weakly electric fish. *J Neurophysiol* 76: 2020–2032, 1996.

Yi TM, Huang Y, Simon MI, and Doyle J. Robust perfect adaptation in bacterial chemotaxis through integral feedback control. *Proc Natl Acad Sci USA* 97: 4649–4653, 2000.

Zucker RS and Regehr WG. Short-term synaptic plasticity. *Annu Rev Physiol* 64: 355–405, 2002.

Downloaded from jn.physiology.org on July 13, 2006